Model-Based Characterization of Homogeneous Metal Plates by Four-Point Alternating Current Potential Drop Measurements

Nicola Bowler, *Senior Member, IEEE,* and Yongqiang Huang, *Student Member, IEEE*

Center for Nondestructive Evaluation, Ames, IA 50011-3042 USA

We determined the conductivity, relative permeability, and thickness of homogeneous metal plates from four-point measurements of alternating current potential drop (ACPD) over the frequency range 1 Hz to 10 kHz. We developed simple analytical expressions from which these parameters can be calculated. In the low-frequency regime, in which the measured voltage tends to a constant, real value, the relative permeability of the plate does not influence the ACPD voltage. For known plate thickness, conductivity can be easily determined, even for ferrous metals. For known conductivity, plate thickness can be determined. Relative permeability can be obtained from measurements at higher frequency, for known conductivity and thickness. The inductance of the pickup circuit can also be determined from higher frequency measurements. This practical technique is especially useful for conductivity or plate thickness measurements in configurations where access is restricted to one side of the plate. We studied brass, aluminum, stainless steel, spring steel, and carbon steel plates. Our results agree with available independent measurements.

***Index Terms*—ACPD, alternating current, complex permeability, conductivity measurement, four-point probe, material characterization, metal plate, permeability measurement, thickness measurement.**

I. Introduction

THE four-point, alternating-current potential difference (ACPD) method measures the potential drop associated with current flowing in a sample, between two points on its surface. If only two wires are used, for both carrying current and measuring potential drop, the contact resistance between the wires and the sample may give rise to significant error. In the four-point method, the potential difference is measured between two additional contact points using a high impedance voltmeter. This means that very little current flows in the measurement circuit and the potential drop across the contact resistance associated with the measuring wires is negligible.

ACPD measurements differ from conventional direct current potential drop (DCPD) measurements since here the time variation of the alternating current gives rise to induction effects in the measurement circuit. These can be accounted for in the theory by including the effect of the electromotance, ε. The electromotance is defined as the integral of the electric field around a loop, in this case the loop of the measurement circuit. In a similar DCPD measurement, the result of this integral is zero. An additional feature of ACPD measurements arises for ferromagnetic samples, in which the relative permeability may be complex and frequency-dependent [1]–[3].

In results presented in this paper, the four-point ACPD method is used to make measurements on a variety of homogeneous metal plates over the frequency range 1 Hz to 10 kHz. Brass, aluminum, stainless steel, spring steel, and carbon steel plates are studied. Using previously derived expressions for the electric field inside the sample and in the region of the probe [4], a simple analytical expression for the ACPD voltage is derived here. The conductivity, relative permeability, and thickness of homogeneous metal plates are determined by adjusting theoretical parameters until the best fit between calculated values and experimental data is obtained. In the low-frequency regime, the measured voltage tends to a constant, real value, which is inversely dependent on both the plate conductivity and thickness. The relative permeability of the plate does not influence the ACPD voltage in the low-frequency regime and, for known plate thickness, the conductivity can be easily determined—even for ferrous metals. Conversely, for known conductivity, plate thickness can be determined. Relative permeability can be obtained from measurements at higher frequency, for known conductivity and thickness. The inductance of the pickup circuit can also be determined from higher frequency measurements. This practical characterization technique requires access to only one side of the plate and, hence, is especially useful for configurations where access to one side of the plate is restricted. Results agree with independent measurements, where available.

II. Theory

The alternating current potential drop (ACPD) method measures the voltage, $\mathcal{V}$, between two pickup points on the surface of a conductor. For the configuration shown in Fig. 1

$$\mathcal{V} = V + \varepsilon = -\int_{(p,y,0)}^{(q,y,0)} \mathbf{E}\cdot d\mathbf{l} + \oint_C \mathbf{E}\cdot d\mathbf{l} \qquad (1)$$

where $\mathbf{E}$ denotes the electric field and C is a closed loop when p' and q' coincide, as is the case when the pickup wires are twisted together at their point of meeting. ε is the rate of change of magnetic flux within the loop. The quantities on each side of (1) are assumed to have harmonic time dependence, of the form $e^{-i\omega t}$. Strictly, the quantities $\mathcal{V}, V, \varepsilon$, and $\mathbf{E}$ appearing in

Digital Object Identifier 10.1109/TMAG.2005.847625

(1) are complex amplitudes. For brevity, the time dependence is not shown explicitly in (1) or in the equations that follow.

In DCPD measurements, there is no induction effect in the measurement circuit ($\varepsilon = 0$), since the current does not vary with time, and the measured potential drop is exclusively due to the conductor. In ACPD measurements, the contribution to $\mathcal{V}$ from the conductor dominates when the frequency is sufficiently low, since the inductive contribution from the measurement circuit, $i\omega L$, is proportional to angular frequency ω. At sufficiently high frequency, the inductive term dominates.

Here, both contributions to $\mathcal{V}$ are evaluated. The far-field approximation for $\mathbf{E}$ is used in calculating $\mathcal{V}$. This approximation gives accurate results when pickup points at $(p, y, 0)$ and $(q, y, 0)$ are sufficiently far from the source points at $(\pm S, 0, 0)$, in practice a few electromagnetic skin depths (δ) in the conductor, where δ is defined

$$\delta = \left(\frac{2}{\omega\mu\sigma}\right)^{1/2} \tag{2}$$

with μ and σ being the magnetic permeability and electrical conductivity of the plate, respectively. In previous work in this area, the functional characteristics of a four-point probe in contact with a conductive half-space were examined theoretically and experimentally [5]. The inductive contribution of the pickup circuit was not considered theoretically, and only the real part of the calculated ACPD voltage was compared with experimental data.

A. Electric Field

For the configuration shown in Fig. 1, the electric field due to alternating current flowing in the two current-carrying wires can be obtained by superposition of fields separately associated with each wire:

$$\mathbf{E}^T(\mathbf{r}) = \mathbf{E}(\mathbf{r}_+) - \mathbf{E}(\mathbf{r}_-) \tag{3}$$

where $r_\pm = \sqrt{(x \pm S)^2 + y^2 + z^2}$. In the following sections, the far-field form of $\mathbf{E}$ is determined in the region of the pickup circuit (air) and in the metal plate for a *single* current-carrying wire located on the axis of a cylindrical coordinate system.

1) Probe Region: For a single wire passing current I into, or out of, a conductive plate, there are two contributions to the electric field in air. One is from the current flowing in the wire, $\mathbf{E}^{\mathrm{w}}$, and the other is from the current density in the plate. In the far-field regime, for the closed loop C, only $\mathbf{E}^{\mathrm{w}}$ is important. Assuming that the wire is perpendicular to the surface of the plate, is infinitesimally thin, and that the current has time-dependence $I(t) = Ie^{-i\omega t}$, the integral form of Ampère's law and then Faraday's law yields

$$\mathbf{E}^{\mathrm{w}}(\rho, z) = \hat{z}\frac{i\omega\mu_0 I}{2\pi}\ln\rho, \quad \rho > 0, \quad z \le 0 \tag{4}$$

where μ_0 is the permeability of free space, ρ is the radial coordinate of a cylindrical system centered on the wire, and $\mathbf{E}^{\mathrm{w}}$ has the same direction as the current density in the wire, $\hat{z}$. The assumption that the wire is infinitesimally thin is reasonable for cases in which the separation of the current wires, $2S$, is much greater than the wire diameter.

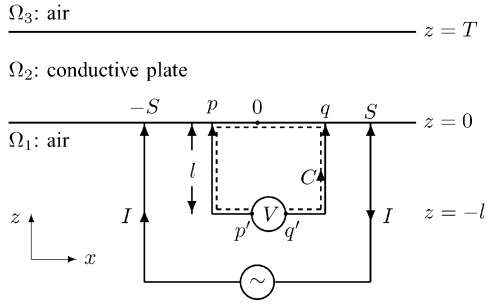

Fig. 1. Four-point probe in contact with a conductive plate. The path of integration, C (- - -), may occupy any plane of constant y. Here, the plane $y = 0$ is shown. l is the dimension of the pickup circuit perpendicular to the conductor surface.

2) Plate: An expression for the electric field in and external to the conductive plate is derived in [4]. For a current source oriented perpendicular to the surface of the plate, only the transverse magnetic potential is required to fully describe the electric field and the problem can be solved in terms of this single, scalar potential.

In the far field, the electric field is dominated by terms of the form e^{ikz}/ρ and

$$E_\rho(\mathbf{r}) = -\frac{ikI}{2\pi\sigma\rho}\sum_{n=0}^{\infty}\left\{e^{ik(z+2nT)} + e^{-ik[z-2(n+1)T]}\right\}, \quad \rho \to \infty, \quad 0 \le z \le T. \tag{5}$$

In (5), $k^2 = i\omega\mu\sigma$. Equivalently, $k = (1+i)/\delta$.

B. Voltage Calculation

Voltage is now calculated according to (1). For the configuration shown in Fig. 1 the contributions are

$$\begin{aligned}\mathcal{V} &= V + \varepsilon \\ &= -\int_p^q E_x^T(x, y, 0)\,dx + \int_0^{-l} E_z^T(p, y, z)\,dz \\ &\quad + \int_{-l}^0 E_z^T(q, y, z)\,dz\end{aligned} \tag{6}$$

with $\mathbf{E}^T$ given by (3). It is a simple matter to evaluate the last two terms on the right-hand side of (6) with E_z given in (4). To neatly evaluate the first term on the right-hand side of (6) recognize that, at the surface defined by $z = 0$, (5) can be written

$$E_\rho(\rho, 0) = -\frac{ikI}{2\pi\sigma\rho}\left[\left(2\sum_{n=0}^{\infty}e^{2iknT}\right) - 1\right], \quad \rho \to \infty. \tag{7}$$

Further [6, eq. (3.6.10)]

$$\sum_{n=0}^{\infty}e^{2iknT} = \frac{1}{1 - e^{2ikT}}$$

so that

$$E_\rho(\rho, 0) = \frac{ikI}{2\pi\sigma\rho}\coth(ikT), \quad \rho \to \infty. \tag{8}$$

The final expression for $\mathcal{V}$ is

$$\mathcal{V} = \frac{I}{4\pi}\left[-\frac{ik}{\sigma}\coth(ikT) + i\omega\mu_0 l\right] \times \ln\left\{\left[\frac{(S-p)^2+y^2}{(S+p)^2+y^2}\right]\left[\frac{(S+q)^2+y^2}{(S-q)^2+y^2}\right]\right\}. \quad (9)$$

The logarithmic term in (9) represents the physical arrangement of the four probe points. For a symmetric, linear probe, $p = -q$ and $y = 0$. Equation (9) reduces to

$$\mathcal{V} = \frac{I}{\pi}\left[-\frac{ik}{\sigma}\coth(ikT) + i\omega\mu_0 l\right]\ln\left|\frac{S+q}{S-q}\right|. \quad (10)$$

From (10) notice that it is the ratio, $a = q/S$, of the position of the pickup point to the position of the source point which is important. Equation (10) can also be expressed

$$\mathcal{V} = \frac{I}{\pi}\left[-\frac{ik}{\sigma}\coth(ikT) + i\omega\mu_0 l\right]\ln\left|\frac{1+a}{1-a}\right|. \quad (11)$$

Similar expressions can be obtained for other symmetric probe configurations, such as a rectangular probe. Here, measurements are made with the probe points arranged in a straight line.

The first term in (9)–(11) is the contribution from the conductor and has real and imaginary parts. The contribution from the measurement circuit is inductive and proportional to the dimension of the circuit perpendicular to the conductor surface, l. It is instructive to analyze the frequency dependence of (11). Various characteristics of the system can be identified.

Expand the term $\coth(ikT)$ making use of the series expansion [6, result 4.5.67]

$$\coth z = \frac{1}{z} + \frac{z}{3} - \frac{z^3}{45} + \cdots, \quad |z| < \pi.$$

Then

$$\mathcal{V} = \frac{I}{\pi}\left[-\frac{1}{\sigma T} + i\omega\mu_0\left(\frac{\mu_r T}{3} + l\right) - \frac{\omega^2\mu^2\sigma T^3}{45} + \mathcal{O}(\omega^3)\right] \times \ln\left|\frac{1+a}{1-a}\right|, \quad f < f_{\mathrm{v}} \quad (12)$$

where μ_r is the relative permeability of the plate, the term $\mathcal{O}(\omega^3)$ represents terms of order ω^3 and higher, and

$$f_{\mathrm{v}} = \frac{\pi}{2\mu\sigma T^2}. \quad (13)$$

Considering the real part of (12), it is apparent that $\mathcal{V}$ obeys the following static formula:

$$\mathcal{V}_{\mathrm{s}} = -\frac{I}{\pi\sigma T}\ln\left|\frac{1+a}{1-a}\right|, \quad f < f_{\mathrm{s}} \quad (14)$$

for all frequencies below a certain threshold frequency, f_{s}, such that

$$\frac{1}{\sigma T} \gg \frac{\omega^2\mu^2\sigma T^3}{45}.$$

Define f_{s} to be the frequency at which the right-hand side, above, is 1% of the left-hand side. Then

$$f_{\mathrm{s}} = \frac{\sqrt{45}}{20\pi\mu\sigma T^2}. \quad (15)$$

TABLE I
PROBE PARAMETERS

probe 1 (brass plate)	
S (mm)	38.2 ± 0.3
q (mm)	9.18 ± 0.01
l (fitted value) (mm)	0.36 ± 0.01
probe 2 (aluminum plate)	
S (mm)	25.4 ± 0.3
q (mm)	9.19 ± 0.01
l (fitted value) (mm)	0.37 ± 0.02
probe 3 (steel plates)	
S (mm)	25.44 ± 0.01
q (mm)	10.15 ± 0.01
l (fitted value) (mm)	0.15 ± 0.01

Considering the imaginary part of (12), it is apparent that the inductance due to the measurement circuit, represented by the parameter l, is negligible in the case that $\mu_r T/3 \gg l$. This is likely to be true for strongly ferromagnetic metals, as shown in Section IV-A.

III. EXPERIMENT

A. Method

ACPD measurements were made as a function of frequency on a range of conductive plates whose properties are discussed in the next section. The plates were mounted on a 5-cm-thick plastic support plate. Electrical contact was made via sprung, point contacts, held perpendicular to the plate surface by being mounted in a plastic support block. In this experiment the four contact points were arranged in a straight line, with a common midpoint between the two current drive points and the two pickup points, such that $p = -q$ (Fig. 1). The dimensions of the probes used are given in Table I. The two current-carrying wires were held perpendicular to the plate surface for a distance of approximately 40 cm above the plate, after which they were twisted together to reduce the effects of interwire capacitance. This distance was sufficient to remove any effect of motion of the current wires on the measured voltage. The two pickup wires were arranged with the objective of minimizing the inductance in the measurement circuit. They ran along the underside of the plastic block housing the pickup contacts, lying as close to the plate surface as possible. They were twisted together at the midpoint between the pickup points.

In the theoretical calculation, two measured values are needed. One is the current through the plate, the other is the voltage measured by the pickup probe. To monitor the current in the plate, a high-precision resistor was connected in series with the drive current circuit and the voltage across the resistor measured. The resistor maintains 1% accuracy over the range of frequency for which it could be measured with an Agilent 4294A precision impedance analyzer; 40 Hz to 40 kHz. The voltage across the resistor and that of the pickup probe were both measured using a Stanford Research Systems SR830 DSP lock-in amplifier. In order to make both voltage measurements using the same lock-in amplifier, a switch was activated by a control signal from the auxiliary analog output of the lock-in amplifier. The current in the plate was maintained as close to 2 A as possible over the frequency range of the experiment. In

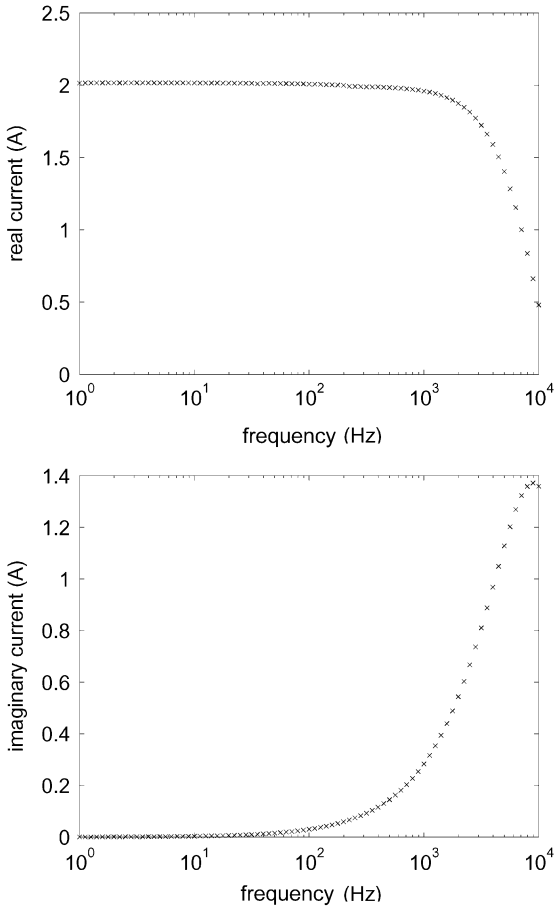

Fig. 2. Measured current in the plate.

practice, the real and imaginary parts of the current varied as shown in Fig. 2.

It was necessary to correct the experimental data for common-mode rejection (CMR) error in the lock-in amplifier. This systematic error shows itself in the fact that, when the pickup terminals are reversed, the measured voltage changes by a few microvolts. The magnitude of the error is, for the nonmagnetic plates, similar to that of the voltage being measured and a corrective procedure is essential. The CMR error was eliminated by taking two sets of measurements, reversing the pickup terminals in between, and averaging.

The drive current was produced by a Kepco bipolar operational power supply/amplifier, model number BOP 20-20M. The sine signal from the internal function generator of the lock-in amplifier was connected to the current programming input of the power supply, with the power supply working as a current drive.

B. Samples

A range of homogeneous metal plates was studied; brass, aluminum, stainless steel, spring steel, and carbon steel. Basic information and parameters of the five plates studied are given in Table II. Details of the alloy types are given below. Conductivities of the brass, aluminum, and stainless steel plates were measured by an eddy-current method. Details of the method are given in the Appendix. The conductivity of the ferrous plates (spring steel and carbon steel) was not measured since, in the eddy-current method, the conductivity and permeability can only be separated at frequencies much lower than 40 Hz, the lower limit of the Agilent 4294A precision impedance analyzer. Standard conductivity meters are incapable of measuring the conductivity of ferrous metals. The fact that the magnetic permeability of the plate does not influence the value of the ACPD voltage in the low-frequency regime, as shown in (14), means that this is a simple and promising method for measurement of conductivity of ferromagnetic metals, which is presently achieved by four-point DCPD measurements on samples whose dimensions must be accurately known.

TABLE II
PLATE PARAMETERS

plate	σ (MSm^{-1})	T (mm)	$w \times l$ (mm)
brass	16.8 ± 0.4	5.66 ± 0.01	615×616
aluminum	20.4 ± 0.4	25.37 ± 0.01	615×616
stainless steel	1.36 ± 0.06	6.36 ± 0.01	457×457
spring steel	-	1.57 ± 0.01	412×412
carbon steel	-	6.30 ± 0.01	616×619

Plate thickness was measured using digital calipers. The horizontal plate dimensions given in Table II, $w \times l$, were sufficiently large that edge-effects were not measurable.

1) Brass: Brass alloy C26000 has nominal composition 70% copper and 30% zinc, according to ASTM B36 standard. According to the mill test report, the specimen examined here had composition 69.62% copper, 0.004% iron, with the remainder being zinc. The plate was supplied by McCaffrey Metal Corp. and was precision ground on receipt to remove surface scratches.

2) Aluminum: The aluminum alloy 7075 plate was supplied by McMaster-Carr in precision-ground form, with dimension tolerance ± 0.13 mm, conforming to ASTM B209 standard. The nominal chemical composition for this alloy is 90.0% aluminum, 1.6% copper, 2.5% magnesium, 0.23% chromium, and 5.6% zinc.

3) Stainless Steel: The type 316 stainless steel plate was supplied by McMaster-Carr in precision-ground form, conforming to ASTM A240 standard. The chemical composition of type 316 stainless steel is given in Table III. Type 316 stainless steel possesses the potential for weak ferromagnetism, with the permeability being related to the amount of martensite present from cold work and the amount of δ-ferrite present due to welding at temperatures which allow the formation of δ-ferrite [8], [9]. In the unworked state, the relative magnetic permeability of type 316 stainless steel is 1.003. This value increases with the percentage of reduction in area due to cold rolling [8], [10]. The precise correlation between magnetic permeability and percent cold reduction is highly sensitive to variations in alloy composition and metallurgical history. This means that wide variations can be observed even among different lots of a given type of stainless steel. For example, after cold rolling to give a 33% reduction in area, a value of $\mu_r = 1.10$ is common [10].

4) Spring Steel: The grade C1074/75 spring steel specimen was supplied by McMaster-Carr in cold-rolled form, completely annealed and conforming to ASTM A684 standard. The chemical composition of alloy C1074/75 spring steel is given in Table III. On receipt, the plate was demagnetized in both

TABLE III
CHEMICAL COMPOSITIONS (WEIGHT %) OF STEELS

	stainless steel [7]	spring steel	carbon steel
chromium	16.0 - 18.0	-	-
nickel	10.0 - 14.0	-	-
carbon	0.08 maximum	0.7 - 0.8	0.15 - 0.20
manganese	2.0 maximum	0.5 - 0.8	0.6 - 0.9
sulfur	0.03 maximum	0.05 maximum	0.05 maximum
molybdenum	2.0 - 3.0	-	-
silicon	1.0 maximum	-	-
phosphorus	0.045 maximum	0.04 maximum	0.04 maximum
iron	remainder	remainder	remainder

horizontal axes using a demagnetizing coil with inner diameter approximately 50 cm.

5) Carbon Steel: The alloy 1018 low-carbon steel specimen was supplied by McMaster-Carr in sheet form. The chemical composition of alloy 1018 low-carbon steel is given in Table III. It was not possible to anneal the specimen on receipt due to its large size. It was attempted to demagnetize the plate point-by-point using a C-core magnet on its surface, again because the plate was too large to fit inside readily available demagnetizing coils. This method is not as reliable as that mentioned above, being likely to leave residual magnetization in local regions of the plate.

C. Standard Error

The standard error in the measurement data is plotted in Fig. 3. This error arises partly due to scatter in the voltage meter and is plate-dependent due to factors such as surface roughness and microstructural variations. The noticeably higher values of the standard error which occur between 200 Hz and 1 kHz are apparently a feature of the instrumentation since the behavior is similar for all plates. Taking the magnitude of the measured voltage into account (next section), the experimental error due to scatter in the data is 1% for the stainless steel and spring steel plates, 2% for the brass and carbon steel plates, and 5% for the aluminum plate.

IV. RESULTS

In Figs. 4 and 5, ACPD measurements are compared with theoretical values, calculated using (11), for brass and aluminum plates. Parameters for the calculation are taken from Table II. The average of ten experimental data sets (taken sequentially) is shown. The value of l was adjusted in the calculation to obtain the best fit to the high-frequency, imaginary part of the data, having negligible influence on the low-frequency data. The physical arrangement of the pickup circuit is such that the pickup wire runs along the underside of the plastic block housing the sprung contacts, near to the plate surface. This means that the minimum possible value of l is half of the wire diameter (since the wire is not infinitesimally thin) although, in practice, an air gap is usually present. The values $l = 0.36$ and 0.37 mm for brass and aluminum, respectively, appear reasonable since the pickup wire is AWG 32 with diameter 0.2 mm and an air gap was observed between the wire and the surface of the plates. The agreement between theory and experiment is very good, except at frequencies between 200 Hz and 1 kHz where the standard error in the experimental data is greater (Section III-C).

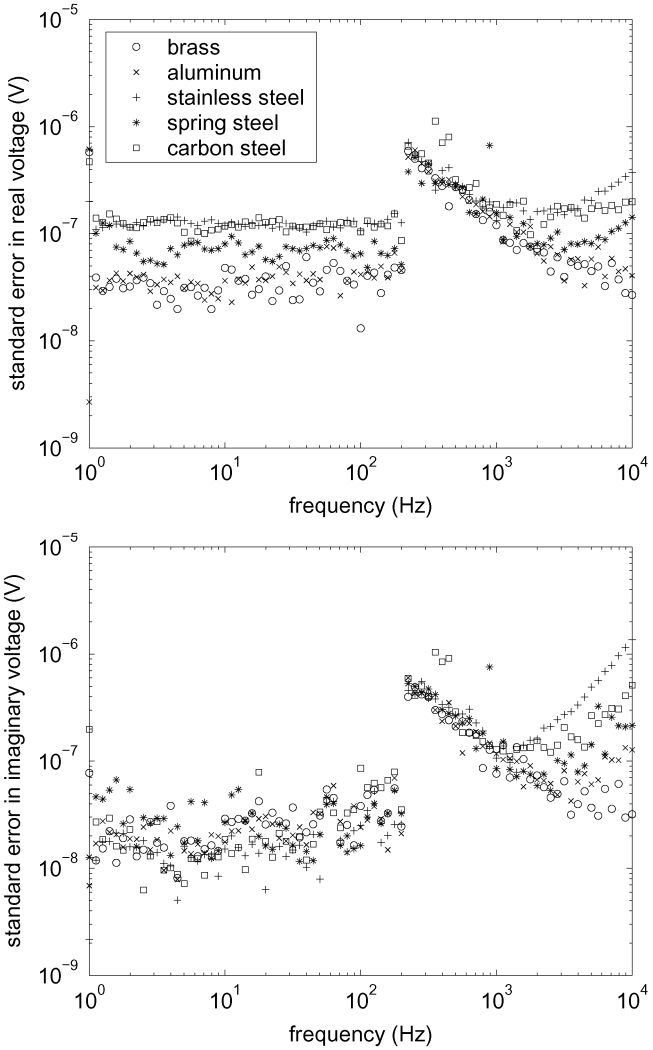

Fig. 3. Standard error in the measured ACPD voltage on each plate.

A. Plate Conductivity and Permeability

In the low-frequency ACPD measurement regime (frequencies $f < f_s$), the real part of the ACPD voltage tends to a constant value and the imaginary part is approximately zero (14). In this regime, the measured voltage is independent of magnetic permeability and the plate conductivity can be deduced from ACPD measurements by finding the best fit between theory and experiment, provided that T is known. Using values for T given in Table II, the value of σ was adjusted in the theory until the root-mean-square (rms) error between calculated voltage values and ACPD measurement data was minimized. The residual rms error was 1% for the brass plate, 4% for the aluminum plate, and 0.1% for the stainless steel plate. The results are shown in Table IV. The errors quoted in Table IV result from combining the random experimental error in the voltage measurement for each plate (Section III-C) with the uncertainty in the amplitude measurement of the voltage meter (1%), the uncertainty in the current measurement (1%) and the uncertainty in the probe parameter a, (11). In probes 1 and 2, the contact points were housed in three separate plastic blocks; one for each of the

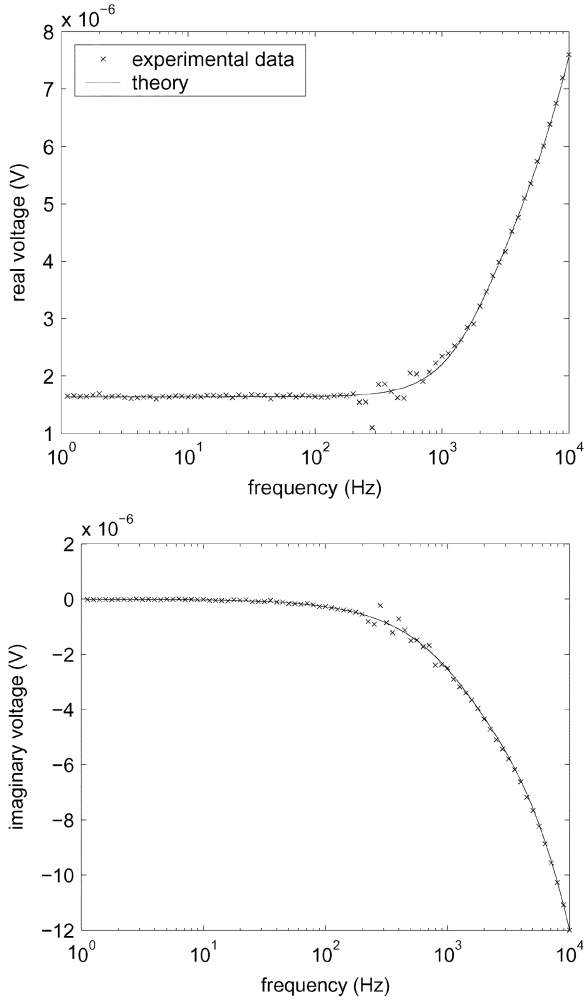

Fig. 4. ACPD measurements on a brass plate compared with theory. Probe 1 was used, with parameters given in Table I. Plate parameters are given in Table II.

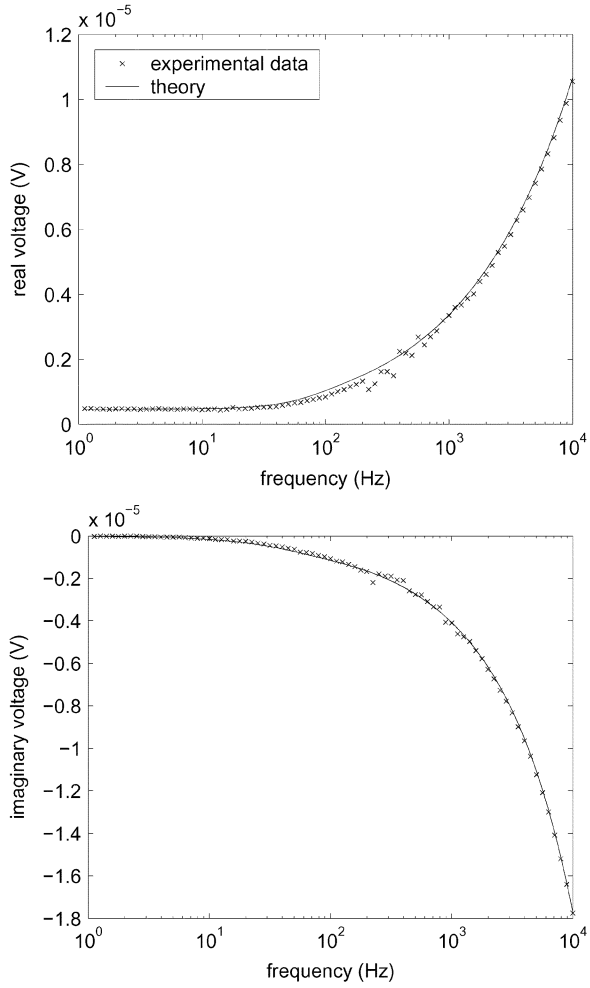

Fig. 5. ACPD measurements on an aluminum plate compared with theory. Probe 2 was used, with parameters given in Table I. Plate parameters are given in Table II.

current input points and one for the two pickup points. For this reason, it was difficult to be precisely sure of the position of the current input points once placed in contact with the plate. The resulting uncertainty in the logarithmic term in (14) is 2%. In probe 3, this uncertainty was made insignificant by housing all four contact points in a single plastic block, permitting measurement of their relative positions by digital calipers. Uncertainty in the measurement of plate thickness was not a significant source of error in the conductivity values determined by ACPD measurements.

The conductivity values obtained by ACPD measurements and those obtained independently by eddy-current measurements, where available, agree within experimental error.

For stainless steel, note that the high frequency real part of the voltage can be used to obtain a value of μ_r, once σ is known from the low-frequency asymptote. For $\sigma = 1.37$ MSm^{-1}, the best fitted value for μ_r is 1.06. This is in accordance with values mentioned in the literature for type 316 stainless steel (see discussion in Section III-B3). Once σ and μ_r have been determined, the high-frequency imaginary part of $\mathcal{V}$, (11), gives the best fit for l as 0.15 mm. This value is somewhat smaller than for probes 1 and 2 (Table I) due to improved probe design. With these parameter values, the curves shown in Fig. 6 are obtained.

TABLE IV
PLATE CONDUCTIVITY AND PERMEABILITY

	eddy-current	ACPD
plate	conductivity, σ (MSm^{-1})	
brass	16.8 ± 0.4	16.7 ± 0.5
aluminum	20.4 ± 0.4	21 ± 1
stainless steel	1.36 ± 0.06	1.37 ± 0.03
spring steel	-	5.5 ± 0.1
carbon steel	-	5.3 ± 0.2
	relative permeability, μ_r	
brass	1	1
aluminum	1	1
stainless steel	1	1.06 ± 0.02
spring steel	-	134 ± 3
carbon steel	-	(281 ± 8) + j(15.1 ± 0.5)

In Fig. 7, theory and experiment are compared for the spring steel plate. From the low-frequency data, 1 to 100 Hz, the conductivity was obtained by minimizing the rms error between the data and theory. From the data between 100 Hz and 10 kHz, μ_r was obtained. The fitted values are shown in Table IV and are in accordance with expectations [11]. Similarly, in Fig. 8, theory and experiment are compared for the carbon steel plate.

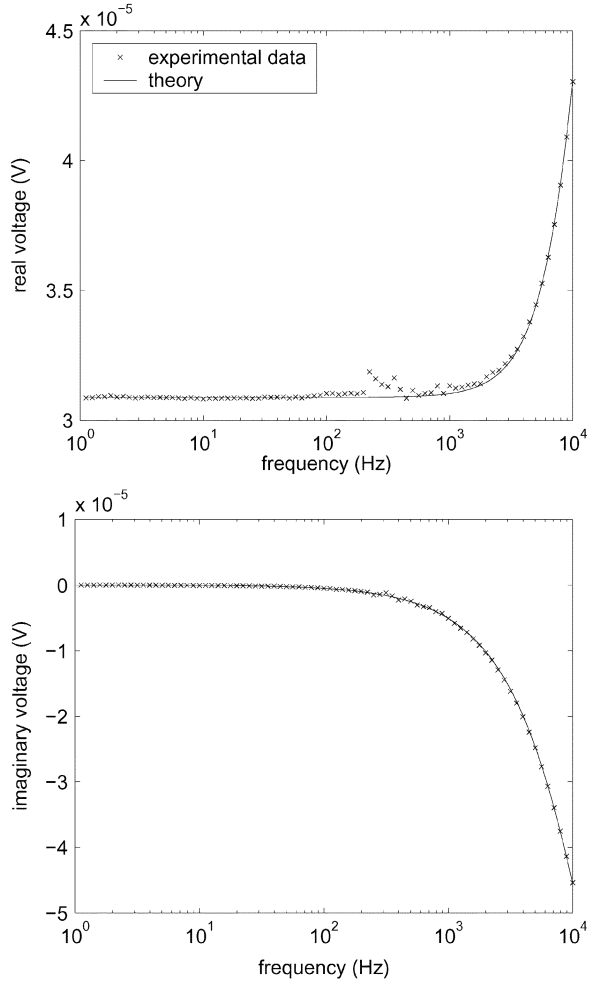

Fig. 6. ACPD measurements on a stainless steel plate compared with theory. Probe 3 was used, with parameters given in Table I. Values for plate conductivity, permeability, and probe self-inductance are obtained from the best fit between theory and experimental data, and are given in Table IV.

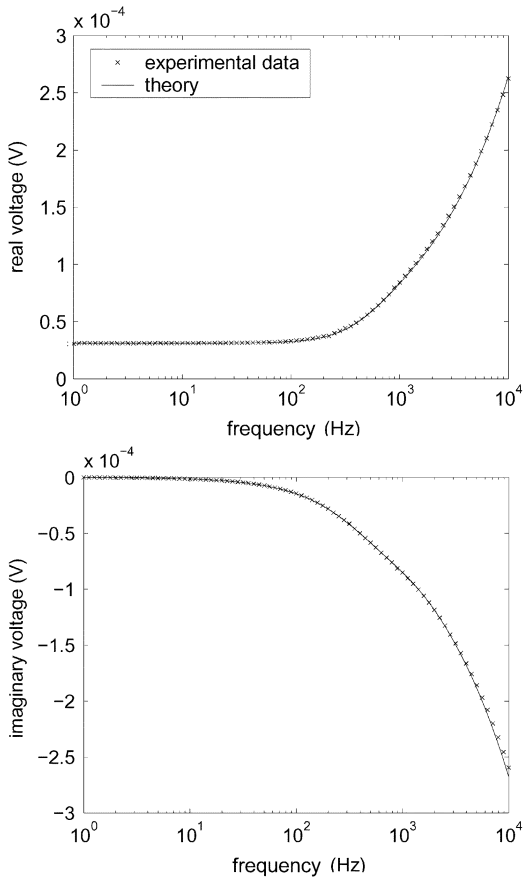

Fig. 7. ACPD measurements on a spring steel plate compared with theory. Probe 3 was used, with parameters given in Table I. Values for plate conductivity and permeability are obtained from the best fit between theory and experimental data, and are given in Table IV.

It was found that a good match between theory and experiment could be obtained up to approximately 100 Hz using a constant, complex value for the relative permeability; $\mu_r^* = 281 + j15.1$. This value is somewhat larger in magnitude than values reported independently in the literature, but the relative proportions of the real and imaginary parts are as observed elsewhere [2]. Above 100 Hz, μ_r^* is evidently frequency-dependent since a good match between theory and experiment cannot be achieved with the restriction that μ_r^* is constant. If desired, the frequency-dependent behavior of μ_r^* may be characterized by matching theory and experiment at each measured frequency, as in [1] and [2]. In the second of these studies, ferrous plates were magnetized in the core of a variable-frequency solenoid. The impedance of a pickup coil wound around the central section of each plate was measured and μ_r^* determined by matching measured and calculated values of the coil impedance. The intensity of the applied magnetic field, the composition, length, and thickness of the plate were all observed to influence μ_r^*. The authors of [1] and [2] explain these observations in terms of a delay in the magnetic induction of the samples with respect to the oscillation of the magnetic field. The phase shift accounts for the complex nature of the magnetic permeability and increases with depth of penetration into the sample. In [2] it is noted that although μ_r^* varies with depth, as well as frequency, it is sufficient for most applications to assume that μ_r^* does not vary with position inside the sample. Some exceptions to this are commercially pure nickel and iron, for which the inductance of an eddy-current coil on thick plates could not be fit to theory for single values of σ and μ_r, but was consistent with a model assuming a thin surface layer with significantly reduced permeability [12]. The difference between the values of permeability measured here for the spring steel and carbon steel plates, despite their similar compositions, may be due to differences in their processing history. For example, the spring steel plate was annealed whereas the carbon steel plate was not. Other contributing factors may be that the spring steel plate was demagnetized by being placed inside a demagnetizing coil, whereas point-by-point demagnetization of the carbon steel plate was attempted due to its large size. Further, the carbon steel plate is several times thicker than the spring steel plate [2].

For each of the plates, the frequency f_s (below which the static formula given in (14) is calculated to be valid) is listed in Table V. f_s is calculated according to (15) using parameters from Table IV. With reference to Figs. 4 to 8 it can be seen that the measured voltages are approximately constant for $f < f_s$, with value $\mathcal{V}_s$ given in (14), as predicted. For the plates studied here, $\mathcal{V}_s$ ranges between approximately 0.5 and 30 μV, as detailed in Table V. According to the discussion at the end of Section II-B,

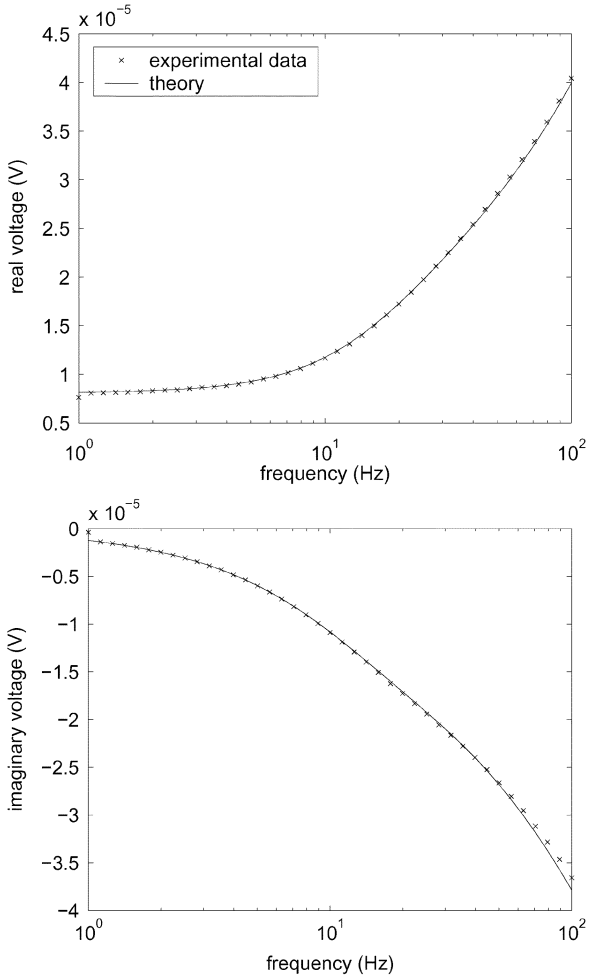

Fig. 8. ACPD measurements on a carbon steel plate compared with theory. Probe 3 was used, with parameters given in Table I. Values for plate conductivity and permeability are obtained from the best fit between theory and experimental data, and are given in Table IV.

the inductance of the measurement circuit is predicted to be negligible for $\mu_r T/3 \gg l$, for $f < f_{\rm v}$, (13). In Table V, the ratio $\mu_r T/(3l)$ is given for each of the plates. From these values, it is evident that inductance in the measurement circuit is influential for the brass, aluminum, and stainless steel plates (the terms differ by approximately one order of magnitude), but is negligible for the strongly ferromagnetic spring steel and carbon steel plates, where the terms differ by two and three orders of magnitude, respectively. For completeness, the frequency below which the series expansion formula (12) is valid, $f_{\rm v}$, is also listed in Table V. In fact, the ratio $f_{\rm v}/f_{\rm s}$ is constant with value $10\pi^2/\sqrt{45} \approx 14.7$.

B. Plate Thickness

In cases where σ is known, the thickness of the plate can be determined by the complement of the procedure for finding σ when T is known, described in the previous section. This is immediately obvious from (14) since, for $f < f_{\rm s}$, $\mathcal{V}$ depends on σ and T in the same way. For the brass, aluminum, and stainless steel plates, values of σ obtained by swept-frequency eddy-current measurements are given in Table II. Taking these as exact, values for the plate thickness were obtained by adjusting the

TABLE V
CHARACTERISTIC FREQUENCIES AND INFLUENCE OF MEASUREMENT CIRCUIT INDUCTANCE

plate	$f_{\rm s}$ (Hz)	$\mathcal{V}_{\rm s}$ (μV)	$f_{\rm v}$ (Hz)	$\mu_r T/(3l)$
brass	158	1.64	2330	5
aluminum	6.46	0.470	94.4	23
stainless steel	1450	30.9	21300	18
spring steel	46.5	31.1	685	580
carbon steel	1.43	8.14	21.1	4900

TABLE VI
PLATE THICKNESS

	thickness, T (mm)	
plate	digital caliper	ACPD
brass	5.65 ± 0.01	5.7 ± 0.2
aluminum	25.37 ± 0.01	25 ± 1
stainless steel	6.36 ± 0.01	6.4 ± 0.3

plate thickness in (14) until the rms error between the experimental data points and the calculated values was minimized. The residual rms error was 2% for the brass plate, 4% for the aluminum plate, and 0.8% for the stainless steel plate. The results are given in Table VI. The errors in the plate thickness quoted in Table VI are computed in a similar way to those in the conductivity (previous section). The most significant sources of error in the ACPD determination of plate thickness are the uncertainty in the measured conductivity of the plates and the standard error in the voltage measurements, Section III-C. Comparing the thickness values with those measured using digital calipers, it is seen that the values agree within experimental error.

Four-point ACPD measurements provide a one-sided method for measuring the thickness of conductive plates provided that the conductivity of the plate is known. The accuracy decreases as plate thickness increases. Here, 4% accuracy for plates approximately 6 mm thick and 5% accuracy for a plate approximately 25 mm thick has been achieved.

V. CONCLUSION

In this paper, a method is presented by which four-point ACPD measurements may be used to characterize homogeneous metal plates. Electrical conductivity, magnetic permeability, and plate thickness are determined by matching the measured frequency-dependent pickup voltage, $\mathcal{V}$, with results calculated from an analytical expression in which $\mathcal{V}$ is expressed in terms of parameters describing the sample and probe. The method is demonstrated for a variety of ferrous and nonferrous metal plates. In future work, effects of the plate edges, cylindrical samples, and the influence of surface layers will be examined.

APPENDIX
EDDY-CURRENT MEASUREMENT OF PLATE CONDUCTIVITY

Conductivities of the brass, aluminum, and stainless steel plates were measured using a procedure similar to that described in [13], outlined here. Swept-frequency measurements of the impedance of a well-characterized, air-cored, eddy-current coil centered on the plates, with coil axis perpendicular to the plate surface, were made over the range 40 Hz to 20 kHz. An Agilent 4294A precision impedance analyzer was used. Measurements

TABLE VII
EDDY-CURRENT COIL PARAMETERS

inner radius (mm)	4.04 ± 0.01
outer radius (mm)	11.4 ± 0.1
length (mm)	8.02 ± 0.01
stand-off (mm)	1.08 ± 0.02
number of turns	1858
self-inductance (mH)	33.9
resonant frequency (kHz)	191

were compared with the theory of Dodd and Deeds [14] and the value of conductivity adjusted in the calculation until the rms error between the calculated values and the measured data was minimized. Following this procedure, the residual rms error was 2% for the brass and aluminum plates and 4% for the stainless steel plate. The uncertainties in the measured conductivity values, stated in Table II, also reflect uncertainties in the values of the coil parameters (Table VII).

Parameters of the eddy-current coil are given in Table VII. The inner radius and length of the coil were determined by measuring the dimensions of the former, using digital calipers, before the coil was wound. Measuring the outer radius of the coil, using digital calipers, yielded a value of 11.84 mm. This physical measurement overestimates the *effective* outer radius of the coil due to the fact that the diameter of the windings is not infinitesimal and the coil is not perfectly wound. Following the procedure given in [13], the effective outer radius of the coil was determined by measuring the coil impedance in air over a frequency range from 40 Hz to 3 kHz and minimizing the rms error between experimental and calculated data (from the theory of [14]) by adjusting the value of the outer radius in the calculation. The value of the outer radius for which the rms error was a minimum was taken to be the effective outer radius of the coil. The effective coil standoff (distance between the base of the coil and the base of the probe casing) was determined similarly, by measuring the coil impedance with the coil placed on an aluminum half-space, over the same frequency range. In principal, similar corrections to the inner radius and length of the coil could be made, but in practice these are insignificant once effective values for the outer radius and standoff have been determined. For further details, see [13].

This conductivity measurement method yields more accurate results for low-conductivity metals than measurements using standard conductivity meters, such as a MIZ-21A eddy current instrument. For this conductivity range, the measurement accuracy of the MIZ-21A is 0.5% IACS.[1] This gives possible errors of 2%, 1%, and 20% in the conductivities of brass, aluminum, and stainless steel, respectively.

ACKNOWLEDGMENT

This work was supported by the National Science Foundation Industry/University Cooperative Research program. The authors would like to thank J. Bowler and M. Johnson for helpful comments regarding the experiment, and T. Theodoulidis for useful discussions and references.

[1]IACS: An abbreviation for International Annealed Copper Standard, a measure of conductivity used to compare electrical conductors to a traditional copper-wire standard. Conductivity is expressed as a percentage of the standard. 100% IACS represents a conductivity of 58 MSm^{-1}.

REFERENCES

[1] V. A. Sandovskii, V. V. Dyakin, and M. S. Dudarev, "Frequency dependence of magnetic permeability in inspection with superposed transducers," *Russ. J. Nondestruct. Test.*, vol. 33, no. 1, pp. 52–55, 1997.

[2] ——, "Frequency dependence of the effective magnetic permeability of plates in homogeneous magnetic field," *Russ. J. Nondestruct. Test.*, vol. 37, no. 11, pp. 757–767, 2001.

[3] J. E. L. Bishop and E. W. Lee, "The behavior of ferromagnetic sheets in alternating electric and magnetic fields I. A domain theory of the skin-effect impedance and complex permeability," *Proc. R. Soc. Lond. A*, vol. 276, pp. 96–111, Dec. 1963.

[4] N. Bowler, "Electric field due to alternating current injected at the surface of a metal plate," *J. Appl. Phys.*, vol. 96, no. 8, pp. 4607–4613, Oct. 2004.

[5] V. A. Mitrofanov, "Problems of the theory of the electric potential method of nondestructive inspection using alternating current," *Russ. J. Nondestruct. Test.*, vol. 34, no. 3, pp. 183–189, 1998.

[6] *Handbook of Mathematical Functions with Formulas, Graphs and Mathematical Tables*, M. Abramowitz and I. A. Stegun, Eds., Dover, New York, 1965.

[7] [Online]. Available: http://www.bosunsupplies.com/StainlessInfo2.cfm

[8] C. V. Dodd and W. A. Simpson, "Measurement of small magnetic permeability changes by eddy current techniques," *Mater. Eval.*, vol. 29, no. 10, pp. 217–221, Oct. 1971.

[9] C. A. Swenson and W. D. Markiewicz, "Magnetic characterization of austenitic stainless steel for nuclear magnetic resonance coils," *IEEE Trans. Appl. Supercond.*, vol. 10, no. 1, pp. 736–739, Mar. 2000.

[10] [Online]. Available: http://www.calweights.com/pdf_files/magnetism.pdf

[11] *CRC Handbook of Chemistry and Physics*, 82nd ed., CRC, London, U.K., 2001. D. R. Lide.

[12] J. C. Moulder, C. C. Tai, B. F. Larson, and J. H. Rose, "Inductance of a coil on a thick ferromagnetic metal plate," *IEEE Trans. Magn.*, vol. 34, no. 2, pp. 505–514, Mar. 1998.

[13] D. J. Harrison, L. D. Jones, and S. K. Burke, "Benchmark problems for defect size and shape determination in eddy-current nondestructive evaluation," *J. Nondestruct. Eval.*, vol. 15, no. 1, pp. 21–34, 1996.

[14] C. V. Dodd and W. E. Deeds, "Analytical solutions to eddy-current probe-coil problems," *J. Appl. Phys.*, vol. 39, no. 6, pp. 2829–2838, May 1968.

Manuscript received August 20, 2004; revised February 18, 2005.

Nicola Bowler (SM'02) was born in Hereford, U.K., on December 6, 1968. She received the B.Sc. degree in physics from the University of Nottingham, Nottingham, U.K., in 1990 and the Ph.D. degree from the University of Surrey, Surrey, U.K., in 1994, for theoretical work in the field of eddy-current nondestructive evaluation (NDE).

Since 1997, she has broadened her interests in theoretical electromagnetics to include dielectric and magnetic behavior of composite materials. She moved to the Center for NDE, Iowa State University, Ames, in 1999.

Yongqiang Huang (S'03) was born in HuNan, China, on August 13, 1973. He received the B.S. degree from North China University of Technology in 1995, the M.S. degree from Tsinghua University in 1998 in automatic control theory and its application, and the Ph.D. degree in electrical engineering from Iowa State University, Ames, in 2004.

He worked as a Network Engineer for China Telecom for more than two years before coming to the United States in 2000 to continue his graduate study.